Mon. Not. R. Astron. Soc. **000**, 1–?? (0000) Printed 16 December 2011 (MN LATEX style file v2.2)

Circumstellar dust as a solution to the red supergiant supernova progenitor problem

Joseph J. Walmswell ⋆, John J. Eldridge
Institute of Astronomy, The Observatories, University of Cambridge, Madingley Road, Cambridge, CB3 0HA

August 2011

ABSTRACT
We investigate the red supergiant problem, the apparent dearth of Type IIP supernova progenitors with masses between 16 and 30 $M_\odot$. Although red supergiants with masses in this range have been observed, none have been identified as progenitors in pre–explosion images. We show that, by failing to take into account the additional extinction resulting from the dust produced in the red supergiant winds, the luminosity of the most massive red supergiants at the end of their lives is underestimated. We re–estimate the initial masses of all Type IIP progenitors for which observations exist and analyse the resulting population. We find that the most likely maximum mass for a Type IIP progenitor is $21^{+2}_{-1}\,M_\odot$. This is in closer agreement with the limit predicted from single star evolution models.

Key words: stars: evolution – supernovae: general – stars: supergiants

1 INTRODUCTION

Nothing in the life of a massive star becomes it like the leaving it. A supernova (SN) is one of the most impressive spectacles that the Universe can afford an astronomer. However, there is some uncertainty as to the range of stars that undergo this most spectacular demise. Observations indicate that stars evolve into red supergiants if their initial masses are between about 12 and 30 $M_\odot$ (Levesque et al. 2006). Stars that are less massive undergo second dredge–up and end their lives as asymptotic giant branch (AGB) stars (Eldridge et al. 2007). Mass–loss rates increase with mass and stars that are more massive suffer enough mass–loss to remove their hydrogen envelopes before they die. They become Wolf–Rayet stars, naked helium stars with thick winds (Crowther 2007). These explode as hydrogen–free Type Ib/c SNe, rather than the more common Type II SNe that are believed to result from the death of red supergiants (Filippenko 1997; Smartt et al. 2009). Type II SNe are in turn divided into Types IIP, IIL, IIn and IIb. Types IIP and IIL are identified by their SN light curves. The former have a plateau and the latter show only a linear decline. The plateau is the result of the photosphere maintaining a constant radius, moving inward in mass as the ejecta expands (Filippenko 1997). This in turn is due to the ionised hydrogen recombining. Type IIb SNe have weak hydrogen lines and light curves similar to hydrogen–free Type Ib SNe, implying that they contain only a small percentage of hydrogen. There seems to be a sequence from Type IIP to Type IIL to Type IIb SNe, driven by increased mass-loss and a consequently reduced mass of hydrogen in the ejecta. Type IIn SNe are distinguished by narrow line hydrogen emission, the result of shock interaction with circumstellar material (Smith et al. 2011). The mass limits have some dependence on metallicity because metal–rich stars have higher mass–loss rates and thus the minimum initial mass of Wolf–Rayet stars is approximately 25 $M_\odot$ at Solar metallicity (Eldridge & Tout 2004). We therefore expect Type II progenitors up to this limit.

The red supergiant problem was first reported by Smartt et al. (2009). They compared 20 Type IIP SN progenitor detections and non–detections with stellar evolution models to determine the minimum and maximum initial mass limits for the progenitors of these SNe. They found that the minimum mass required for stars to explode as Type IIP SNe was $8.5^{+1}_{-1.5}\,M_\odot$, which is consistent with the observed upper limit for white dwarf formation (Weidemann & Koester 1982; Williams et al. 2009). More surprisingly, they found an upper limit of $16^{+1.5}_{-1.5}\,M_\odot$, a 95 per cent confidence upper limit of 21 $M_\odot$. In essence, the red supergiant problem is that this estimate is well below the maximum mass estimated for red supergiants. There therefore appears to be an absence of higher–mass red supergiant SN progenitors, leaving the fate of stars with masses between 16 and 25-30 $M_\odot$ uncertain.

It should be mentioned that the alternative to deducing masses from progenitor models is to model the supernova directly. This has the advantage of not requiring

⋆ E-mail: jjw49@ast.cam.ac.uk

pre–explosion images, although it does depend on detailed follow–up observations of the supernova itself. Utrobin and Chugai have used a one–dimensional hydrodynamic code (Utrobin 2004) to model the SNe 2005cs (Utrobin & Chugai 2008) and 2004et (Utrobin & Chugai 2009). Both have detected progenitors and in this paper we deduce initial masses of 9^{+1}_{-4} and $12^{+1}_{-1}\,M_\odot$ respectively. This compares with 18 and $28\,M_\odot$ for the hydrodynamic masses. If these masses are correct, the red supergiant problem ceases to be. However, three earlier independent attempts to model the progenitor of 2005cs gave masses of $9^{+3}_{-2}\,M_\odot$ (Maund et al. 2005), $10^{+3}_{-3}\,M_\odot$ (Li et al. 2006) and between 6 and $8\,M_\odot$ (Eldridge et al. 2007), a discrepancy noted by the authors. There are other approaches; Dessart & Hillier (2011) have constructed models that include the nebula phase of the supernovae, which is more amenable to detailed simulation. These SNe modelling approaches have great potential but wait on more sophisticated models.

Another approach is to consider the ratios of the different types of SNe. One then integrates the initial mass function (IMF) to find the limits that provide the desired number of stars. Smith et al. (2011) considered the fractions of core collapse SNe from the Lick Observatory Supernova Search (LOSS) and observed that the proportion of Type Ib/c SNe was much too high for all of them to be the result of single star evolution. In addition, with the standard Salpeter IMF, the observed fraction of Type IIP SNe was such that it could be produced by single stars with initial masses in the range $8.5 - 13.7 M_\odot$. These facts imply that binary interaction allows the production of hydrogen–free progenitors at lower masses than would otherwise be the case. Smith et al. (2011) suggest that if binaries are included the upper limit for red supergiants would be in the range of 18 to 24 $M_\odot$.

However, this study found a lower fraction of Type IIP SNe than previous work. The core collapse SNe broke down as 48 per cent Type IIP and 22 per cent Type Ib/c, compared with 59 and 29 respectively for the survey of Smartt (2009). The reason for this is not clear. Smartt (2009) considered a 28 Mpc volume–limited survey using all detected SNe within that volume, whereas Smith et al. (2011) used 60 Mpc and only those SNe detected in LOSS. Type IIP SNe tend to be dimmer than other types so those at large distances may have been missed. While these selection effects were accounted for, such adjustments are, by their nature, very uncertain. Another reason for the difference could be that Smith et al. (2011) had more complete spectroscopic and light curve follow-ups and so had greater accuracy in their classifications.

It is possible to obtain the required SNe fractions with an appropriately chosen stellar population. Eldridge et al. (2011) showed that a population composed of a mixture of binary and single stars could explain the rates of Smartt et al. (2009). Smith et al. (2011) used their own binary population models to explain their results. The uncertainity in the rates means that it is hard to use these fractions to tightly constrain the progenitor mass range, particularly when the shape of the IMF means that small changes in the lower limit result in large changes in the population fractions. In contrast large changes in the upper limit result in small changes in the population fractions. Hopefully future surveys will resolve the discrepancy.

If we accept the existence of the red supergiant problem then we must consider a number of possible explanations. First, that these massive red supergiants form black holes with faint or non–existent SNe (e.g. Heger et al. 2003). Secondly, that their envelopes are unstable and eject a large amount of mass pre–SN (e.g. Yoon & Cantiello 2010). Thirdly, that they explode as a different type of SN (e.g. Kotak & Vink 2006). We suggest a fourth explanation, that the mass estimates may be systematically inaccurate at the high–mass end. Mass estimates are based on mass–luminosity relations, so extra intrinsic extinction close to the red supergiant progenitors would give reduced luminosities and hence lower predicted masses. Smartt et al. (2009) were careful to provide extinction estimates when possible from measurements of nearby supergiants and from the supernova itself. These could be underestimates. If red supergiants produce extra dust local to the star, it would be destroyed in the supernova explosion. This is very plausible. It is known that red supergiants form dust in their winds (Massey et al. 2005). Furthermore, IR interferometry has shown that this dust can be found very close to the star itself (Danchi et al. 1994). Smith et al. (2011) also suggest dust as a solution to the red supergiant problem.

In this work, we first describe the theoretical models from which we derived mass–magnitude relations. We then show how these were used to deduce masses from a population of Type IIP SN progenitors. Finally, we deduce the most probable upper and lower mass limits and present our conclusions.

2 SIMULATING RED SUPERGIANTS

We begin by considering the Cambridge STARS code, the source of our stellar models. These models were processed to generate observed colours with the BaSeL V3.1 model atmosphere grid (Westera et al. 2002) and the relevant broad–band filter functions. We used the dust production rate observed by Massey et al. (2005) to estimate the amount of circumstellar extinction that would then manifest. This allowed the calculation of mass–magnitude relations both with and without the inclusion of circumstellar dust. We also consider the nature of dust production, including non–spherical behaviour.

2.1 The Cambridge STARS code

The Cambridge STARS code was originally developed by Peter Eggleton in the 1960s (Eggleton 1971). It uses a non–Lagrangian mesh, where the mesh function ensures that the points are distributed so that no quantity of physical interest is allowed to vary by a large amount in the intervals. The code has been gradually improved and updated and the work in this paper is based on the code described by Stancliffe & Eldridge (2009) and those referenced by them.

Convection is included in the code by the mixing length theory of Böhm-Vitense (1958), with a solar–calibrated mixing length parameter of $\alpha = 2.0$. Convective overshooting is obtained with the method of Schrder et al. (1997), with an overshooting parameter of $\delta_{\rm OV} = 0.12$. This method involves the addition of a δ term to the adiabatic gradient, allowing mixing to occur in regions that are weakly stable by the

Schwarzchild criterion. The code follows the chemical evolution of ^{1}H, ^{3}He, ^{4}He, ^{12}C, ^{14}N, ^{16}O and ^{20}Ne, together with structural variables.

We use the mass–loss scheme described by Eldridge & Tout (2004). For main–sequence OB stars the mass–loss rates are calculated according to Vink et al. (2001) and for all other stars we use the rates of de Jager et al. (1988), where the metallicity scaling goes as $(z/z_{\odot})^{0.5}$. This theory is older but the the rates have been recently tested for red supergiants and been shown to be still the best rates available for them (Mauron & Josselin 2011).

We have created a library of evolution models, with values of Z, the metallicity fraction by mass, equal to 0.02, 0.01, 0.008 and 0.006. These cover the metallicity range of the IIP progenitors given by Smartt et al. (2009). The fractions of hydrogen and helium were determined on the assumption of constant helium enrichment from the primordial condition of X=0.75, Y=0.25 and calibrating to a Solar composition of X=0.70, Y=0.28 and Z=0.02, i.e. that $Y = 0.25 + 1.5Z$. We evolve our models through to core neon burning, a few years before core collapse.

2.2 The colour–magnitude diagrams

The Cambridge STARS code outputs the physical parameters for a stellar model at each time–step. These include the bolometric luminosity and the surface temperature. Because the stellar observations are in the form of colours and magnitudes, either the luminosity and the surface temperature must be estimated from the observations or a method of calculating colours and magnitudes from the models must be developed. We choose the latter course because this requires fewer assumptions. Smartt et al. (2009) used the opposite approach and, for that reason, the masses they deduced sometimes differ by a small amount. We use the method described by Eldridge & Stanway (2009) to process the code output and calculate magnitudes to compare to those observed. The BaSel v3.1 grid of model atmospheres is arranged over surface temperature and effective gravity. Using the values of these variables from the code, we obtained appropriate templates for the SEDs for each model at each time–step. We then applied the filter functions to extract the magnitudes in the various bands. This allowed us to produce colour–magnitude diagrams from the evolution tracks.

To check the validity of our synthetic colours we compared our models to red supergiants observed in the Magellanic Clouds by Levesque et al. (2006) and in the Milky Way by Levesque et al. (2005). These observations included estimates for the total extinction based on spectrophotometric modelling, so it was possible to process the data to get the absolute colours and magnitudes in the absence of extinction. This meant that the models did not yet have to take into account the effects of circumstellar extinction. This is shown in Figure 1. We see that the models agree well with the observations, with the red supergiants appearing towards the end of the evolution tracks and ranging in mass between about 10 and 30 $M_{\odot}$. Some of the SMC stars are cooler than predicted and may have higher metallicities. This is not unexpected with a large and heterogeneous population.

To test the validity of the models further, we took the

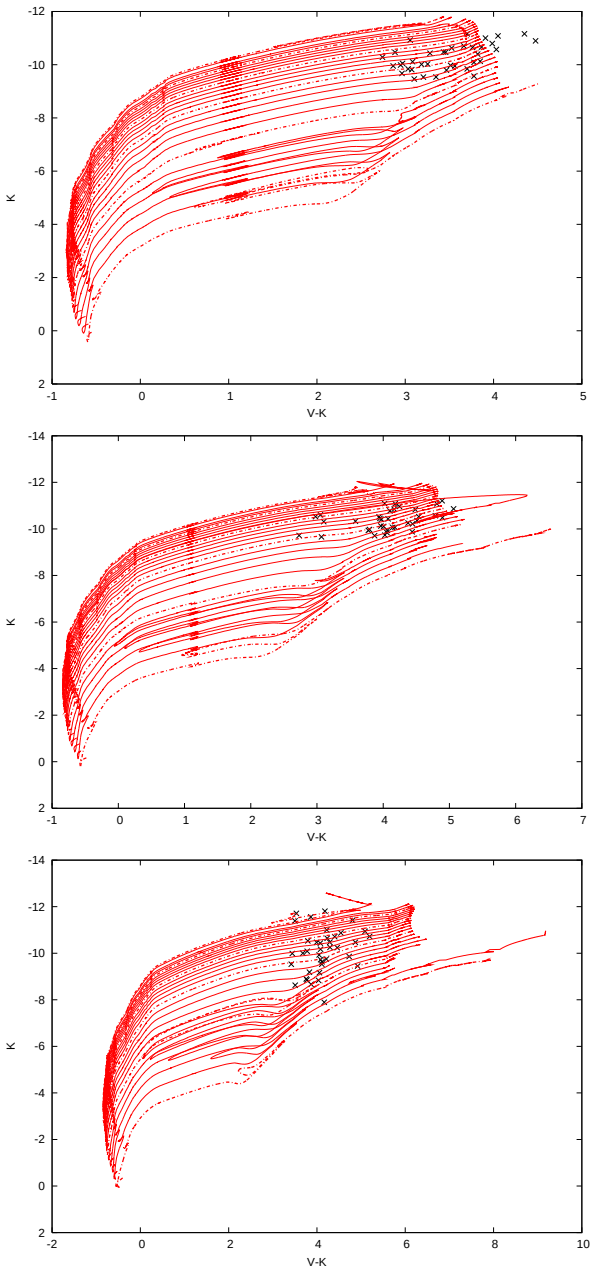

Figure 1. Evolution tracks for every integer mass between 5 and 30 $M_{\odot}$, with the multiples of 5 indicated by dashed lines. The crosses are the observed red supergiants. The SMC stars are at the top and the models use $Z = 0.004$. The LMC stars are in the middle and the models use $Z = 0.01$. The Milky Way stars are at the bottom and the models use $Z = 0.02$.

data and made cumulative frequency plots in M_K. We made similar plots from the models by first identifying which stars became red supergiants during their lifetimes. We required that $V - K > 2.5$ so as to get the reddest stars. The lower limit in K was set to be -9.5 for the Clouds models and -8.5 for the Galactic models. These limits are reasonable for red supergiants and were chosen to reflect the distribution of the observations. We weighted the K magnitudes by the timestep to reflect a greater probability of observation, and the Salpeter IMF. We used metallicities of $Z = 0.004$ for the

SMC, $Z = 0.01$ for the LMC and $Z = 0.02$ for the Galactic population. The comparison is shown in Figure 2.

The agreement is quite good, although there are fewer very luminous stars in the LMC and SMC sets than this simple application of our models predicts. This is probably because all three data sets were not compiled to reflect a stellar population but as an observationally convenient group of red supergiants. In addition, because we weight by the timestep and the IMF only, we are implicitly assuming a constant rate of star formation, a doubtful supposition. We have only considered single stars and binary interactions may change these predicted synthetic frequencies (Eldridge et al. 2008) and we may be underestimating the mass–loss rates of the most luminous red supergiants (Yoon & Cantiello 2010).

2.3 Circumstellar dust

When the surface temperature of a red supergiant falls below about 5000 K, dust begins to condense out of the stellar wind at a distance of around $5 - 10\mathrm{R_{star}} \approx 1000 R_{\odot}$ (Massey et al. 2009a). It might be expected that the amount of dust production would correlate with the mass–loss, which in turn correlates with the luminosity, because this is responsible for the stellar wind (van Loon et al. 2005). Massey et al. (2005) showed that the dust production rate correlates with the bolometric luminosity, with a least squares fit of $\log_{10}(\dot{\mathrm{M}}_{\mathrm{dust}}) = -0.43\mathrm{M_{bol}} - 12.0$, where the dust production rate has units of $\mathrm{M}_{\odot}$/year.

The dynamics of the wind and the dust is complicated and simulations indicate an absence of spherical symmetry. Woitke (2006) found that various instabilities such as Rayleigh–Taylor or Kelvin–Helmholtz lead to the formation of arcs and caps of dust despite the spherical initial conditions. This means that one would expect variation in the observed mass–loss and extinction that is entirely due to the behaviour of the dusty wind along the line of sight. This cannot be accounted for with the STARS code, because in the absence of observations of the dust, one can only use the relation between the luminosity and the dust production to estimate an average extinction. The additional variation due to the lack of spherical symmetry means an additional source of uncertainty.

The amount of extinction that is due to circumstellar dust depends on the past history of the star, which has a continuous loss of mass over time. In contrast, the STARS code calculates the properties of the stars at intervals determined by the time–step. To account for this, we calculated the launch velocity of the dust and the dust–production rate for each time in the output data. This, together with the stellar radii, when interpolated, gave the distribution of dust with distance from the star. Following Massey et al. (2005) we begin by referring to Whittet (2003) who showed how the extinction owing a thin shell of dust can be determined. If one assumes a dust grain density of $s = 2500\,\mathrm{kg\,m^{-3}}$, applicable to low-density silicates and a refractive index of $m = 1.50$, one can obtain the extinction A_V in terms of the path length L.

$$\rho_d = (3.7 \times 10^{-8}) s \frac{m^2 + 2}{m^2 - 1} \frac{A_V}{L}. \quad (1)$$

After the substitutions are made, one obtains the density in terms of the path length and the extinction only.

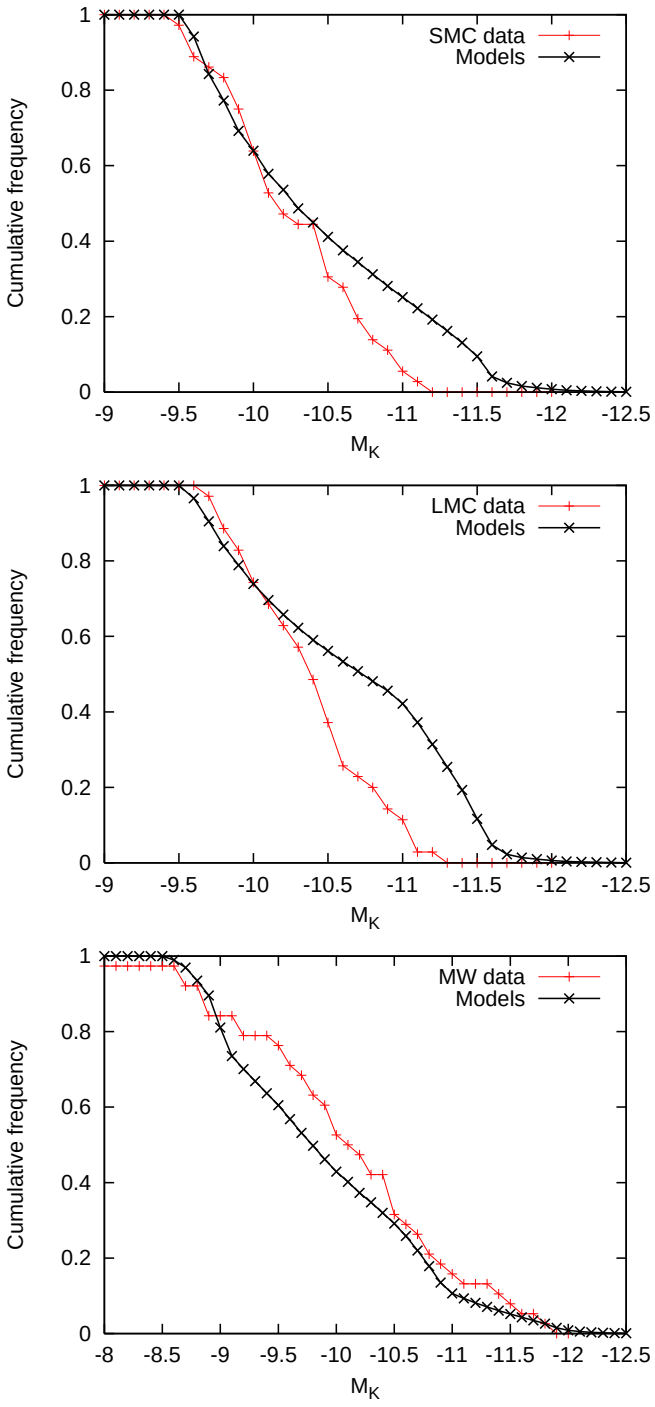

Figure 2. The cumulative frequency diagrams, in K band magnitude, for red supergiants observed in the SMC, the LMC and the Milky way. They are compared with cumulative frequency curves from synthetic populations derived from the same models used for Figure 1

$$\rho_d = (3.1 \times 10^{-4}) \frac{A_V}{L}. \quad (2)$$

If a thin shell of dust is used, the thickness of the shell δR cancels with the path length. The extinction caused by the shell is then in terms of the dust mass M_d and the radius R.

Table 1. Extinction at standard and HST pass–bands relative to the V band, as given by Cardelli et al. (1989).

Filter	A_λ/A_V
U	1.569
B	1.337
V	1.000
R	0.751
I	0.479
J	0.282
H	0.190
K	0.114
F555W	0.996
F606W	0.885
F814W	0.597

$$A_V = \frac{(3.2 \times 10^3) L M_d}{4\pi R^2 \delta R}. \quad (3)$$

$$A_V = \frac{(3.2 \times 10^3) M_d}{4\pi R^2}. \quad (4)$$

The dust was modelled as a series of these thin shells, over which the total extinction was integrated at each timestep. The A_V was then used to calculate the extinction in the other pass–bands by using the extinction law and associated ratios described in Cardelli et al. (1989). These are shown in Table 1.

The density of dust falls off according to an inverse square law as each shell moves outwards in the stellar wind. Therefore only material very near to the star has a significant effect. We find about 95 per cent of the extinction is due to material closer than $50\,R_{star}$ in all the models. This means that the dust is unlikely to affect the SN because it is rapidly swept up and destroyed in the explosion. The inverse square law also means that the distance at which dust first forms in the wind is important. We chose to set this to $10\,R_{star}$, an upper estimate, to ensure that our extinctions are modest underestimates.

3 THE SUPERNOVA PROGENITORS

We use the compilation of SN detections and non–detections of Smartt et al. (2009). All progenitor information can be found in that paper and the references therein. We supplement this with SN 2009md (Fraser et al. 2011a).

The metallicities are based on neighbouring O/H number ratios, where $[\mathrm{O/H}] = \log_{10}(\mathrm{O/H}) + 12$. For $[\mathrm{O/H}] > 8.7$, the $Z = 0.02$ models were used. Similarly, for $8.5 < [\mathrm{O/H}] \leqslant 8.7$, $Z = 0.01$, for $8.4 < [\mathrm{O/H}] \leqslant 8.5$, $Z = 0.008$ and for $8.2 < [\mathrm{O/H}] \leqslant 8.4$, $Z = 0.006$. This is a more precise division by metallicity than was possible for Smartt et al. (2009). Errors are given, when known, and the errors for the absolute magnitude were obtained by combining the other errors in quadrature.

We assigned masses to the progenitors by comparing the absolute magnitudes, together with their error bars, with a plot of red supergiant final luminosities against initial mass. We decided to plot the minimum and maximum magnitudes in the lifetime of our theoretical red supergiants, the lifetime being between the end of core helium burning and the termination of the model. This gave a range in luminosity over which a star of a given initial mass might explode. Masses were first obtained from the original models and again after processing to include the effects of circumstellar dust. The error in the magnitudes gave the error in the masses.

Figure 3 shows how the predicted magnitudes for the $Z = 0.02$ models varies with initial mass in the V, R, I, and K bands. As expected, dust is much more of a problem at shorter wavelengths, when extinction is more severe, and at higher masses, when mass–loss is greater.

However, although extinction is less important at longer wavelengths, changes in stellar luminosity have more of an effect. When a red supergiant becomes more luminous, most of this increase in output is at longer wavelengths. One can see from Figure 3 that the difference between the minimum and maximum magnitudes for a given mass is highest in the K band. This is particularly acute for the lower masses because they end core helium burning as blue supergiants, setting a very low minimum magnitude in the infrared.

The lower–mass models also have higher maximum magnitudes than the extrapolation of the behaviour of the more massive stars might predict. These stars undergo second dredge–up, becoming more luminous asymptotic giant branch (AGB) stars (Eldridge et al. 2007). In both cases, increasing the magnitude range also increases the uncertainty in the progenitor mass–luminosity relation. Finally the sharp increase in the maximum V magnitude at the high mass end indicates incipient Wolf–Rayet star formation.

3.1 The non–detections

For the non–detections, no progenitor was confidently identified in the pre–images. This still provides useful information because it sets a limit on the magnitude of the progenitor. If the star were brighter, it would have been detected. If the errors in the magnitudes are approximately normal, there is an 84 per cent probability that the magnitude of the non–detected progenitor is less than the upper error bar. This is a sufficiently high confidence level that we took the upper mass limit to be the lowest mass with a magnitude range entirely brighter than this upper error bar.

Some of the SNe had non–detections in several pass–bands. The magnitude limits quoted in Table 2 are those which gave the lowest upper mass limit. The other pass–bands merely set a higher upper mass limit which added no additional information. If we compare the mass limits deduced from the dustless models with those with dust we can see that the difference between the two increases with mass. Most notably that for SN 2003ie changes from 22 to $25\,/\mathrm{M}_\odot$.

3.2 The detected progenitors

The actual detections are fewer in number than the non–detections. For progenitors observed in multiple bands, a mass for each band was calculated and these were averaged. For SN 2009bk Mattila et al. (2008) used the progenitor SED to deduce a total extinction of $A_V = 1.0 \pm 0.5$ and the absolute magnitudes take this into account. Because this includes any extinction from circumstellar dust, there was no need to use the dusty models and the predicted mass is the same in both cases.

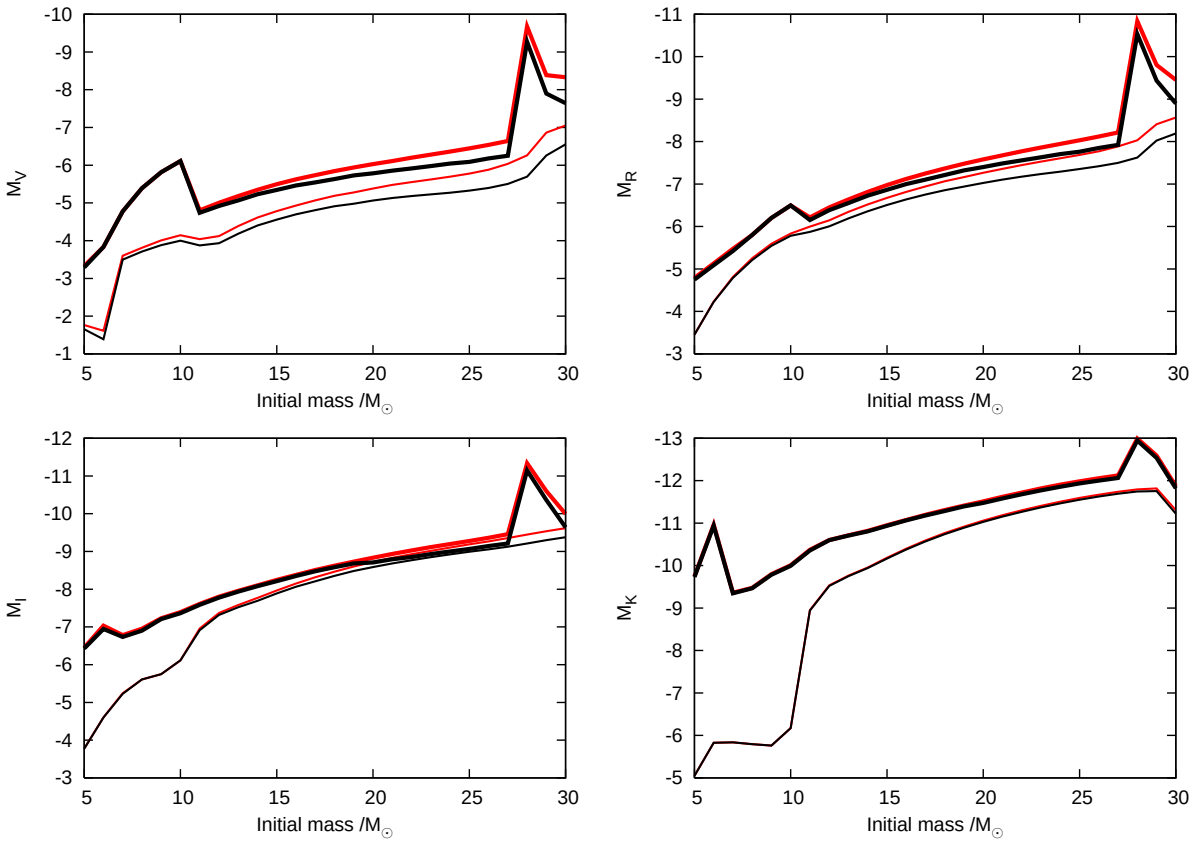

Figure 3. The final magnitudes in V, R, I, and K from our Z=0.02 stellar models. Red indicates the dust free models and black the models with dust. The thinner lines are for the minimum magnitudes and the thicker are for the maximum magnitudes.

Table 2. The observed parameters and estimated upper mass limits for Type IIP supernova progenitors that were not detected in pre–explosion images. We include the masses without considering extinction due to intrinsic dust, $M_{dustless}$, and the masses taking intrinsic dust into account M_{dust}. Note that we consider 2004A to be a non–detection. The observation of a progenitor was doubtful.

SN	Metallicity /dex	Distance /Mpc	Apparent magnitude	Absolute magnitude	$M_{dustless}$ /$M_\odot$	M_{dust} /$M_\odot$
1999an	8.3	18.5±1.5	$m_{F606W} > 24.7 \pm 0.2$	$M_{F606W} > -7 \pm 0.3$	18	21
1999br	8.4	14.1±2.6	$m_{F606W} > 24.91$	$M_{F606W} > -5.89 \pm 0.4$	11	12
1999em	8.6	11.7±1.0	$m_I > 22.0$	$M_I > -8.5 \pm 0.2$	18	19
1999gi	8.6	10.0±0.8	$m_{F606W} > 24.9 \pm 0.2$	$M_{F606W} > -5.7 \pm 0.3$	12	13
2001du	8.5	18.2±1.4	$m_{F814W} > 24.25$	$M_{F814W} > -7.4 \pm 0.2$	13	13
2003ie	8.5	15.5±1.2	$m_R > 22.65$	$M_R > -8.3 \pm 0.2$	22	25
2004A	8.3	20.3±3.4	$m_{F814W} > 24.25$	$M_{F814W} > -7.4 \pm 0.2$	14	15
2004dg	8.5	20.0±2.6	$m_{F814W} > 25.0$	$M_{F814W} > -6.9 \pm 0.3$	11	11
2006bc	8.5	14.7±2.6	$m_{F814W} > 24.45$	$M_{F814W} > -6.8 \pm 0.5$	11	12
2006my	8.7	22.3±2.6	$m_{F814W} > 24.8$	$M_{F814W} > -7.0 \pm 0.2$	11	11
2006ov	8.9	12.6±2.4	$m_{F814W} > 24.2$	$M_{F814W} > -6.3 \pm 0.4$	10	11
2007aa	8.4	20.5±2.6	$m_{F814W} > 24.44$	$M_{F814W} > -7.2 \pm 0.3$	12	13

3.3 Other deduced masses

Table 4 lists the properties of SNe 2004am and 2004dj, both of which are Types IIP but lack detected progenitors. Smartt et al. (2009) describe how population synthesis codes were used to deduce progenitor masses from their parent clusters. These SNe were part of the survey and are included for completeness.

3.4 The maximum likelihood limits

The masses for the detections and non–detections have been drawn from a distribution of Type IIP progenitors with unknown parameters. If we assume that the progenitors are drawn from a population described by the initial mass function (IMF), the nature of the IMF and the range of masses which explode as Type IIP SNe are the important parameters. Following the method of Smartt et al. (2009), we used

Table 3. The observed parameters and estimated masses for Type IIP supernovae that were detected in pre–explosion images. We include the masses without considering extinction by intrinsic dust, $M_{dustless}$, and the masses taking intrinsic dust into account, M_{dust}.

Supernova	Metallicity /dex	Distance /Mpc	Apparent magnitude	Absolute magnitude	$M_{dustless}$ /$M_\odot$	M_{dust} /$M_\odot$
1999ev	8.5	15.14±2.6	$m_{F555W} = 24.64 \pm 0.17$	$M_{F555W} = -6.7 \pm 0.4$	18^{+3}_{-3}	20^{+6}_{-4}
2003gd	8.4	9.3±1.8	$m_V = 25.8 \pm 0.15$	$M_V = -4.47 \pm 0.5$	8^{+2}_{-1}	8^{+2}_{-2}
			$m_I = 23.13 \pm 0.13$	$M_I = -6.92 \pm 0.4$		
2004et	8.3	5.9±0.4	$m_I = 22.06 \pm 0.12$	$M_I = -7.4 \pm 0.2$	11^{+1}_{1}	12^{+1}_{-1}
2005cs	8.7	8.4±1.0	$m_I = 23.48 \pm 0.22$	$M_I = -6.3 \pm 0.3$	9^{+1}_{-4}	9^{+1}_{-4}
2008bk	8.4	3.9±0.5	$m_I = 22.20 \pm 0.19$	$M_I = -7.2 \pm 0.4$	12^{+2}_{-4}	12^{+2}_{-4}
			$m_H = 18.78 \pm 0.11$	$M_H = -9.4 \pm 0.3$		
			$m_K = 18.34 \pm 0.07$	$M_K = -9.7 \pm 0.3$		
			$m_J = 19.50 \pm 0.06$	$M_J = -8.7 \pm 0.3$		
2009md	9.0	21.3±2.2	$m_V = 27.32 \pm 0.15$	$M_V = -4.63^{0.3}_{-0.4}$	8^{+4}_{-2}	8^{+5}_{-2}
			$m_I = 24.89 \pm 0.08$	$M_I = -6.92^{+0.4}_{-0.3}$		

Table 4. The observed parameters and estimated masses for Type IIP supernovae that have mass estimates derived from observations of their host clusters.

SN	Metallicity /dex	Distance /Mpc	Apparent magnitude	Absolute magnitude	M_{nodust} /$M_\odot$	M_{dust} /$M_\odot$
2004am	8.7	3.7±0.3	n/a	n/a	12^{+7}_{-3}	n/a
2004dj	8.4	3.3±0.3	n/a	n/a	15^{+3}_{-3}	n/a

maximum likelihood theory to find parameters that gave the greatest probability of generating the data. If P_i is the probability of the ith detection or non–detection being made, the likelihood $\mathcal{L}$ is the probability of observing the whole dataset.

$$\mathcal{L} = \prod_{i=1}^{i=N} P_i(m). \quad (5)$$

Taking the natural logarithm converts the product into a sum and simplifies matters because maximising $\log_e \mathcal{L}$ is equivalent to maximising $\mathcal{L}$.

$$\log_e \mathcal{L} = \sum_{i=1}^{i=N} \log_e[P_i(m)]. \quad (6)$$

For the non–detections, the probability of the event is the probability that a randomly chosen star has a mass between the lower limit and the detection limit. Thus we integrate the IMF between these limits and normalise. The IMF is generally assumed to be describable by a power law for supersolar masses. Here γ is the index such that the the default Salpeter law gives $\gamma = -1.35$. The parameters to be varied are m_{min}, the lower mass mass limit and m_{max}, the upper mass limit.

$$P_i \propto \int_{m_{min}}^{m_i} m^{\gamma-1} dm. \quad (7)$$

$$P_i = \frac{m_{min}^{\gamma} - m_i^{\gamma}}{m_{min}^{\gamma} - m_{max}^{\gamma}}. \quad (8)$$

The detection limits m_i are the 84 per cent confidence limits. The probability of non detection if m_i exceeds m_{max} is 1 and the probability if m_i is less than m_{min} is 0.16.

For the detections, the probability of the event is the probability that a star has this deduced mass subject to the errors. The distribution of the errors is unclear and the simplest way of accounting for the uncertainty is to integrate the IMF between the upper and lower limits set by the errors. However, this skews the distribution towards lower masses. We follow Smartt et al. (2009) by instead integrating the IMF from the upper limit to the predicted mass and then in a straight line from the value of the IMF at the predicted mass to zero at the lower limit. If the upper error mass m_{i+} exceeds m_{max} then the integral is truncated at m_{max}. Similarly if the lower error mass m_{i-} is less than m_{min} then the integral is truncated at m_{min}.

The maximum likelihood values are of little interest without some measure of how probable alternatives are. To do this the confidence regions must be determined. For two parameters we have the 68, 90 and 95 per cent confidence regions when $\chi = 2.3, 4.6, 6.2$ (Press et al. 1992).

$$\ln \mathcal{L}_{max} - \ln \mathcal{L} = \frac{1}{2}\chi. \quad (9)$$

We calculated the maximum likelihood contours when both the upper and lower limits are varied. Initially we used only the detections. The non–detections favour arbitrarily low values for the lower limit because the slope of the IMF makes low–mass stars more probable. Then, with the lower limit fixed from the detections, the non–detections were included to see what effect they had on the upper limit.

The contrast between the two models is shown in Figure 4. The models without dust predicted an upper limit of $18^{+2}_{-2} M_\odot$ and a 95 per cent confidence limit of 25 $M_\odot$. However, the dust models give $21^{+2}_{-1} M_\odot$ and, more significantly, a 95 per cent limit of more than 30 $M_\odot$. This means that we can no longer say with certainty that there is population

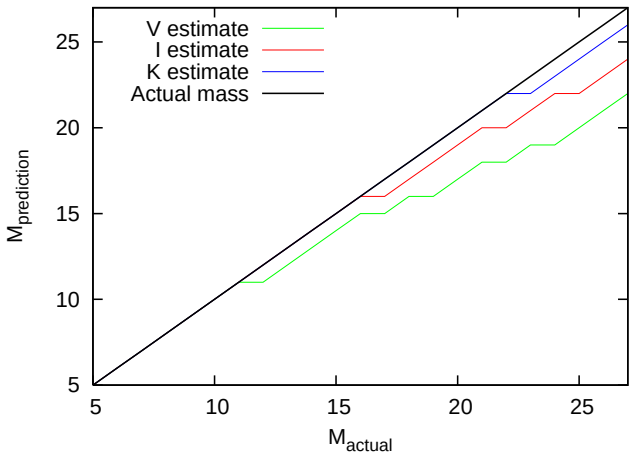

Figure 6. Actual compared with deduced initial masses of red supergiants for theoretical observations in V, I, and K. Models are from the $Z = 0.02$ series.

of red supergiants that do not end as Type IIP SNe. This upper limit is consistent with that obtained by modelling the population of SN progenitors and accounting for binary evolution, i.e. Smith et al. (2011) and Eldridge et al. (2011).

In Figure 5, we present plots of the deduced initial masses of the progenitors with and without dust, in order of increasing mass. They are contrasted with the curves representing a population of stars following the Salpeter distribution, with upper limits of 16.5 and 25 $M_{\odot}$. In both cases the lower limit is 8.5 $M_{\odot}$. It should be noted that SN 1999ev, the most massive progenitor, undergoes the greatest change in predicted mass when dust is considered, from 18^{+3}_{-3} to 20^{+6}_{-4} /$\mathrm{M}_{\odot}$. No other star is more influential in deducing the upper limit and our results will be more certain when we have more similarly massive stars.

Recently a progenitor to SN 2009kr was identified (Fraser et al. 2011b) but it is not clear yet whether it is a single or a binary star, a Type IIP or a Type IIL (Elias-Rosa et al. 2010). If it is a single star, the observations of $\mathrm{M_V} = -7.6 \pm 0.6$ and $\mathrm{M_V} - \mathrm{M_I} = 1.1 \pm 0.25$ imply initial masses of $21^{+3}_{-4}\mathrm{M}_{\odot}$ and $23^{+4}_{-5}\mathrm{M}_{\odot}$ from the models without and with dust. However, the star is more of a yellow supergiant and may have evolved through the red supergiant phase (Elias-Rosa et al. 2010), in which case our models would not be appropriate.

4 DISCUSSION

We have presented evidence that the red supergiant problem is caused by aliasing of the higher masses. This is illustrated in Figure 6 where we have plotted the initial mass of red supergiants at solar metallicity against the mass that would be deduced if we were to take the magnitudes of the dust–extincted models and compare them with the mass–luminosity relation from the models without dust.

The model for circumstellar dust is fairly crude, based on a best fit between luminosity and dust production from which there is considerable deviation. It generates an average extinction of never more than about $1\,\mathrm{A_V}$, whereas observations have revealed stars with several times that value (Massey et al. 2005).

Detailed models of dusty winds have shown that they do not maintain spherical symmetry but form transient cap structures (Woitke 2006). This implies that that the amount of extinction varies with the line of sight and over time. This variability was observed by Massey et al. (2009b), who found an average change of 0.5 mag in the V band in a sample of red supergiants in M31. This change occurred after only three years. Significantly, there was no change in the K band, strongly implying that the change in the magnitudes was driven by variable extinction. It is also likely that dust production varies with metallicity but we have not taken this into account.

The main achievement of our dust model is to show that, even with an unnaturally unvarying but realistic amount of dust production, the red supergiant problem ceases to be. The increased extinction of the higher–mass models introduces such uncertainty into the observations as to make it impossible to confidently set an upper mass limit lower than 25–30 $\mathrm{M}_{\odot}$, the red supergiant upper limit.

The upper mass limit could be determined more precisely by obtaining more pre–explosion images in the infrared, where the effect of extinction is much less. Alternatively, good spectroscopy of the detected progenitors could be used to calculate the total extinction. This would require waiting for one of the relatively small number of nearby well–studied red supergiants to explode. Models of the SNe themselves are also likely to yield more progenitor masses in the future and recent work in that direction has been encouraging (Dessart & Hillier 2011). Until then the uncertain but significant circumstellar extinction means that we do not need to look for alternatives to Type IIP SNe for the death of red supergiants.

ACKNOWLEDGEMENTS

JJW and JJE would like to thank the anonymous referee for their suggestions. They have led to a much improved paper. JJW thanks the STFC for his studentship and JJE is supported by the IoA's STFC theory rolling grant. The authors would also like to thank Stephen Smartt and Christopher Tout for discussion and comments.

REFERENCES

Böhm-Vitense E., 1958, ZAp, 46, 108
Cardelli J. A., Clayton G. C., Mathis J. S., 1989, ApJ, 345, 245
Crowther P. A., 2007, ARAA, 45, 177
Danchi W. C., Bester M., Degiacomi C. G., Greenhill L. J., Townes C. H., 1994, AJ, 107, 1469
de Jager C., Nieuwenhuijzen H., van der Hucht K. A., 1988, A&As, 72, 259
Dessart L., Hillier D. J., 2011, MNRAS, 410, 1739
Eggleton P. P., 1971, MNRAS, 151, 351
Eldridge J. J., Izzard R. G., Tout C. A., 2008, MNRAS, 384, 1109
Eldridge J. J., Langer N., Tout C. A., 2011, MNRAS, 692

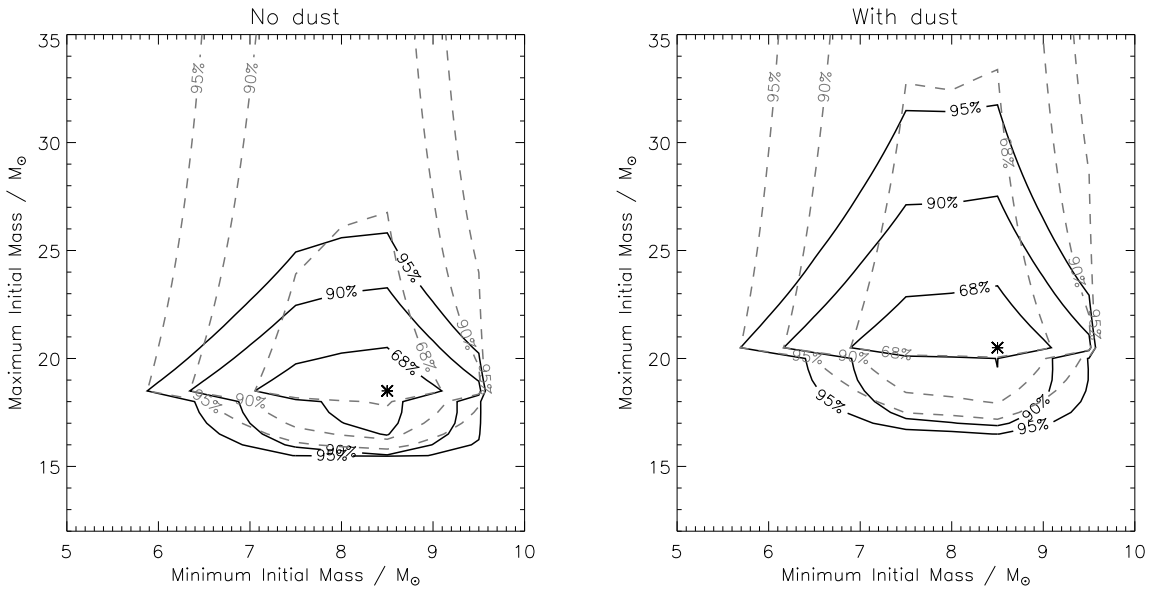

Figure 4. Maximum likelihood contours. The dashed lines are for the detections only and the solid are when the non–detections are included.

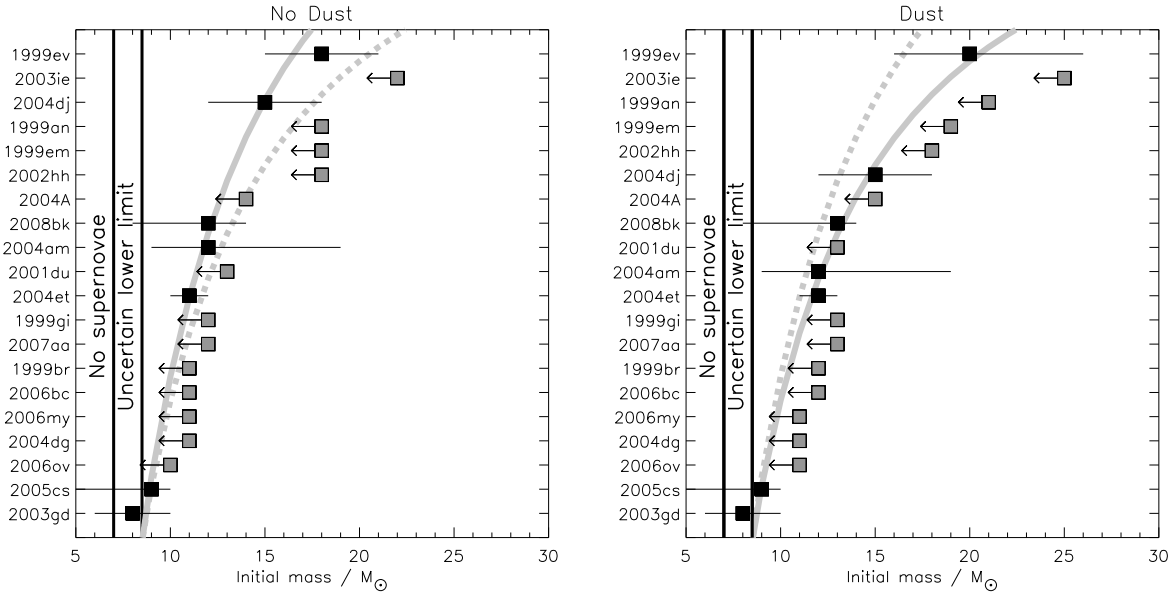

Figure 5. Diagram showing the derived masses of progenitors compared to the expected mass distribution if the maximum Type IIP SNe progenitor mass is 16.5 $M_\odot$ or 25 $M_\odot$.

Eldridge J. J., Mattila S., Smartt S. J., 2007, MNRAS, 376, L52

Eldridge J. J., Stanway E. R., 2009, MNRAS, 400, 1019

Eldridge J. J., Tout C. A., 2004, MNRAS, 353, 87

Elias-Rosa N., Van Dyk S. D., Li W., Miller A. A., Silverman J. M., Ganeshalingam M., Boden A. F., Kasliwal M. M., Vinkó J., Cuillandre J.-C., Filippenko A. V., Steele T. N., Bloom J. S., Griffith C. V., Kleiser I. K. W., Foley R. J., 2010, ApJl, 714, L254

Filippenko A. V., 1997, ARAA, 35, 309

Fraser M., Ergon M., Eldridge J., Valenti S., Pastorello A., Sollerman J., Smartt S. J., Agnoletto I., Arcavi I., Benetti S., Botticella M.-T., Bufano F., Campillay A., Crockett R. M., Gal-Yam A., Kankare E., Leloudas G., Maguire K., Mattila S., Maund J., Salgado F., Stephens A., Taubenberger S., Turatto M., 2011a, MNRAS (in press), arXiv 1011.6558

Fraser M., Takats K., Pastorello A., Smartt S. J., Mattila S., Botticella M.-T., Valenti S., Ergon M., Sollerman J., Benetti S., Bufano F., Crockett R. M., Danziger I. J., Maund J. R., Taubenberger S., Turatto M., 2011b, ApJ, 714, L280

Heger A., Fryer C. L., Woosley S. E., Langer N., Hartmann D. H., 2003, ApJ, 591, 288

Kotak R., Vink J. S., 2006, A&A, 460, L5
Levesque E. M., Massey P., Olsen K. A. G., Plez B., Josselin E., Maeder A., Meynet G., 2005, ApJ, 628, 973
Levesque E. M., Massey P., Olsen K. A. G., Plez B., Meynet G., Maeder A., 2006, ApJ, 645, 1102
Li W., Van Dyk S. D., Filippenko A. V., Cuillandre J.-C., Jha S., Bloom J. S., Riess A. G., Livio M., 2006, ApJ, 641, 1060
Massey P., Plez B., Levesque E. M., Olsen K. A. G., Clayton G. C., Josselin E., 2005, ApJ, 634, 1286
Massey P., Plez B., Levesque E. M., Olsen K. A. G., Silva D. R., Clayton G. C., 2009a, ASP, 3
Massey P., Silva D. R., Levesque E. M., Plez B., Knut A. G., Geoffrey O., Clayton C., Meynet G., Maeder A., 2009b, ApJ, 703, 420
Mattila S., Smartt S. J., Eldridge J. J., Maund J. R., Crockett R. M., Danziger I. J., 2008, ApJl, 688, L91
Maund J. R., Smartt S. J., Danziger I. J., 2005, MNRAS, 364, L33
Mauron N., Josselin E., 2011, A&A, 526, A156+
Press W. H., Teukolsky S. A., Vetterling W. T., Flannery B. P., 1992, Numerical Recipes in fortran. The Art of Scientific Computing, 2nd edn. Cambridge Univ. Press
Schrder K. P., Pols O. R., Eggleton P. P., 1997, MNRAS, 285, 696
Smartt S. J., 2009, ARAA, 47, 63
Smartt S. J., Eldridge J. J., Crockett R. M., Maund J. R., 2009, MNRAS, 395, 1409
Smith N., Li W., Filippenko A. V., Chornock R., 2011, MNRAS, 412, 1522
Stancliffe R. J., Eldridge J. J., 2009, MNRAS, 396, 1699
Utrobin V. P., 2004, Astron. Lett., 30, 293
Utrobin V. P., Chugai N. N., 2008, A&A, 491, 507
—, 2009, A&A, 506, 829
van Loon J. T., Cioni M.-R. L., Zijlstra A. A., Loup C., 2005, A&A, 438, 273
Vink J. S., de Koter A., Lamers H. J. G. L. M., 2001, A&A, 369, 574
Weidemann V., Koester D., 1982, A&A, 121, 77
Westera P., Lejeune T., Buser R., Cuisinier F., Bruzual G., 2002, A&A, 381, 524
Whittet D. C. B., 2003, Dust in the Galactic Environment. Bristol: IOP
Williams K. A., Bolte M., Koester D., 2009, ApJ, 693, 355
Woitke P., 2006, A&A, 452, 537
Yoon S., Cantiello M., 2010, ApJl, 717, L62